



Experimental investigation of laser surface texturing and related biocompatibility of pure titanium

Haoyu Li¹ · Xin Wang² · Junjie Zhang¹ · Binyu Wang² · Marina Breisch³ · Alexander Hartmaier⁴ · Igor Rostotskiy⁵ · Vyacheslav Voznyy⁵ · Yu Liu^{2,6}

Received: 21 October 2021 / Accepted: 7 January 2022 / Published online: 17 January 2022
© The Author(s), under exclusive licence to Springer-Verlag London Ltd., part of Springer Nature 2022

Abstract

While pure titanium is a material of choice for medical applications for its excellent mechanical and chemical properties, further improving its surface-related functionalities by surface texturing is also promising. In the present work, we experimentally investigate the fabrication, as well as the resulting functionalities of surface wettability and biocompatibility, of precise mesh-type surface textures on pure titanium by picosecond pulsed laser ablation operating at 1064 nm wavelength. Specifically, the dependence of microgroove morphology on average power and scanning speed is evaluated to yield optimized laser processing parameters, which are utilized to fabricate high precision mesh-type surface textures with uniform feature size and limited thermal effects on pure titanium. Subsequent performance evaluation tests demonstrate that the mesh-type surface textures induce a beneficial effect on the biocompatibility with respect to BMSC cells due to the enhanced hydrophilicity.

Keywords Pure titanium · Laser surface texturing · Mesh-type texture · Wettability · Biocompatibility

1 Introduction

Pure titanium has been widely used in fields of aerospace, marine engineering, transportation and biology, owing to its excellent properties such as light weight, high specific strength, stable structure, excellent corrosion resistance and

biocompatibility [1]. While the application of pure titanium requires high stability in mechanical, physical and chemical properties, enhancing the surface functionalities by various surface treatment techniques is essentially desired for promoting the performance of pure titanium-based parts. While the performance of surface coating technology is limited by fracture and delamination of coated thin films [2], and the mechanical processing technology for difficult-to-machine materials is suffering from the severe tool wear [3], laser surface texturing (LST), in which regular surface textures or patterns are fabricated through laser ablation, has been proven as a promising method of surface treatment for a wide variety of materials due to its advantages of low cost, high efficiency and high quality [4–7].

In particular, the effectiveness of LST in enhancing the surface functionalities of titanium and its alloys has been well demonstrated. On the side of friction and wear, Durairaj et al. fabricated micro-textures on the rake face of tungsten carbide cutting tools, which are found to be effective in alternating cutting force, shear angle, contact area and adhesion in orthogonal cutting of aluminum [4]. Wang et al. fabricated surface textures with different shapes, pitches and widths on Ti-6Al-4V (TC4) and reported that the fabricated textures significantly improve the tribological properties of the titanium alloy under

✉ Junjie Zhang
zhjj505@gmail.com

✉ Yu Liu
rainfall1982@163.com

¹ Center for Precision Engineering, Harbin Institute of Technology, Harbin 150001, China
² Department of Laboratory, Fourth Affiliated Hospital of Harbin Medical University, Harbin 150001, China
³ BG University Hospital Bergmannsheil Bochum, Ruhr-University Bochum, Bochum 44789, Germany
⁴ Interdisciplinary Centre for Advanced Materials Simulation, Ruhr-University Bochum, Bochum 44801, Germany
⁵ V. Bakul Institute for Superhard Materials National Academy of Sciences of Ukraine, Kyiv 04074, Ukraine
⁶ Department of Blood Transfusion, the Fourth Affiliated Hospital of Harbin Medical University, Harbin 150001, China

oil lubrication conditions [8]. Kümme et al. fabricated linear groove textures with a width of 30 μm and a depth of 10 μm on TC4 and found that the surface texturing leads to a reduction up to a factor of 160 in friction coefficient and wear compared to non-textured surface [9]. Xu et al. fabricated circular pits with a depth of 7.777 μm and an area occupancy ratio of 19.6% on TC4, which are effective in lowering friction coefficient and wear compared with non-textured surface [10]. On the side of wettability, Cunha et al. found that the anisotropy of LST textured TC4 surface is a key factor in controlling the wetting behavior [11]. Li et al. found that groove textures fabricated on TC4 can only prompt the wettability for the groove spacing larger than 0.25 mm [12]. MacDonald et al. reported that the roughening of pure titanium surface by surface texturing can reduce contact angle accompanied with improved its hydrophilicity [13]. On the side of corrosion, Conradi et al. fabricated groove textures on TC4 to improve the corrosion resistance [14]. Xu et al. found that the corrosion resistance of textured TC4 surfaces is improved by increasing the texture density [15]. On the side of biocompatibility, Zhou et al. reported that the groove textures on TC4 by LST significantly improved the bio-functionalization of titanium alloy, in terms of cell adhesion, cell growth and contact guidance [16]. Kumari et al. found that the distribution of cells on the textured TC4 surface is preferentially along the roughness peak area of texture edge or cavity, and the cells tend to be distributed on the edge of the texture as a whole [17]. Cunha et al. cultured human mesenchymal stem cells (hMSCs) on the textured TC4 surface to explore their abilities to differentiate into osteoblasts. Their results showed that the cell area and focal adhesion area are lower on the textured surfaces than that on the polished surface. However, after a longer period of culture, the matrix mineralization and bone-like nodule formation on the textured surface are enhanced. It is thus believed that the textured surface is beneficial for the differentiation of hMSCs into the osteoblast lineage [18].

However, previous research on LST of titanium and its alloys is mainly focused on TC4, and the LST of pure titanium is rather limited. On the one hand, pure titanium has higher elastic modulus, plasticity, corrosion resistance, wear resistance and biocompatibility than TC4, and accordingly possesses higher potential in medical application than TC4 [19, 20]. Thus, further enhancing surface functionalities of pure titanium by LST is also promising. On the other hand, laser ablation-based microstructure fabrication is a process of melting, vaporizing and recasting of the material, which means that the thermodynamic properties of ablated materials have an important

influence on the precision of fabricated surface textures [21]. In particular, pure titanium has lower thermal conductivity and linear expansion coefficient than TC4 [22, 23]. Consequently, the laser processing parameters of TC4 established in previous work may not be suitable for processing pure titanium, and it is necessary to investigate the dependence of pure titanium surface textures on laser processing parameters. Finally, the textures fabricated in most of previous work are grooves and circles with low area occupancy ratio [24–26]. While the area occupancy ratio is an important parameter that affects surface contact area, how to increase the area occupancy ratio by utilizing different geometries of textures is critical to improve the performance of surface textures.

Therefore, in the present work we carry out experimental studies on the LST and related functionalities of wettability and biocompatibility of pure titanium. Firstly, effects of laser processing parameters of average power and scanning speed on the precision of ablated groove morphology are investigated. Secondly, high-precision mesh-type textures are fabricated on pure titanium using the optimized laser processing parameters. Finally, effect of the fabricated textures on the surface wettability and biocompatibility of pure titanium is addressed.

2 Methodology

2.1 Material

In this work, commercially available TA2 pure titanium samples are used, which have a size of 10 mm in length, 10 mm in width and 0.6 mm in thickness. The chemical composition of TA2 pure titanium is listed in Table 1. Prior to LST, pure titanium samples are sequentially grinded by abrasive papers with 80, 180, 400, 800, 1000, 1200, 1500 and 2000 grits to remove the oxide film on the surface, which finally results into a surface roughness (R_a) of 0.2 μm . Then, the ground samples are cleaned in an ultrasonic cleaning machine for 20 minutes, followed by drying in a closed cabinet. And the dried samples are further polished to reach a surface roughness of 0.025 μm . Note that the samples after grinding and polishing are sequentially subjected to ultrasonic cleaning in liquid mixed with acetone, absolute ethanol and deionized water for 20 minutes at a temperature of 25°C, aiming for removing oxides and contaminations before the LST experiments.

Table 1 Chemical compositions of TA2 pure titanium.

Element	Ti	Fe	C	N	O	H
Composition(%)	Residual	0.033	0.011	0.01	0.12	0.001

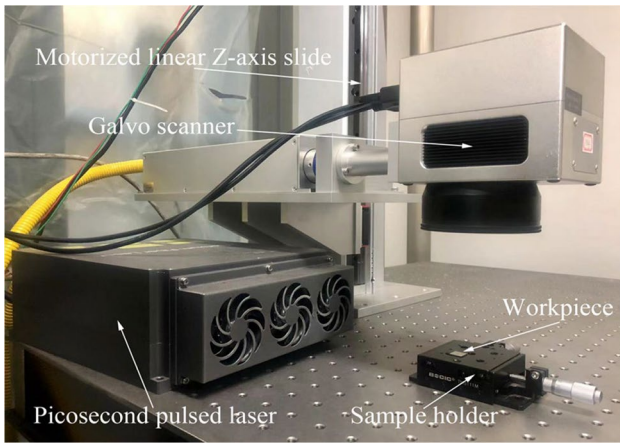


Fig. 1 Experimental configuration of LST device

2.2 Experimental setup of LST

The LST experiments are carried out using a laser micromachining device shown in Fig. 1, which is composed of a picosecond pulsed laser, a galvo scanner, a motorized linear Z-axis slide with a motion accuracy of 5 μm and a sample holder. The picosecond pulsed laser has a pulse width of 150 ps, a wavelength of 1064 nm, a laser beam diameter of 30 μm and a repetition frequency range of 60–1200 kHz.

In the LST process, the horizontally polarized Gaussian laser beam is firstly precisely focused onto the pure titanium surface, accompanied by precisely adjusting the focusing length through the movement of vertical Z-axis slide. The focusing length is 100 mm for a laser beam diameter of 30 μm. After the focusing of laser beam on the sample surface, the designed surface textures are then implemented in the software of Ezcad2 for laser marking. And the laser processing parameters such as average power and scanning speed are also controlled by the software.

The area occupancy ratio is an important parameter that affects the functionalities of surface textures. Pratap and Patra [27] investigated the type of texture geometry on the surface wettability and tribological properties of textured TC4 and found that the micro-mesh textures with an intermediate pitch of 200 μm and a depth of 30 μm possess higher reduction in coefficient of friction under all the loads and sliding velocities than the micro-dimple textures, due to higher wettability and Vickers micro-hardness accompanied by the higher area occupancy ratio. Thus, in the present work a mesh-type texture

with a width of 60 μm, a depth of 30 μm and a pitch of 200 μm is considered. After LST, the surface texture morphology is characterized by optical microscopy and scanning electron microscope (SEM), and the surface texture profile is characterized by white light interferometer.

2.3 Experimental setup of surface wettability testing

In order to investigate the effect of surface texture on the wettability of pure titanium, surface wettability of textured sample (Ti-tex) and non-textured sample (Ti) is evaluated by the sessile drop measurement, which is performed at room temperature using as two testing media of distilled-deionized (DD) water and Modified-Simulated Body Fluid (m-SBF). The m-SBF is designed to have an ion concentration close to human blood plasma, and the composition is listed in Table 2. Prior to the measurements, the samples are ultrasonically cleaned first with ethanol for 5 minutes and then, dried at room temperature. In the sessile drop measurement, droplets of testing media with a volume of 2 μL are successively deposited on sample surface with a micrometric syringe for 60 s. The droplet profile is analyzed by using the axisymmetric drop shape analysis-profile (ADSA-P) method [28], and the static contact angle is estimated by fitting the Laplace equation to the experimental profiles. Three repeat measurements are made for the same position to ensure the accuracy of data acquisition.

2.4 Experimental setup of biocompatibility testing

In order to investigate the effect of surface texture on the biocompatibility of pure titanium, biocompatibility of textured sample (Ti-tex), non-textured sample (Ti) and control group is evaluated by culturing BMSC on the sample surface in vitro. The control group is the culture plate without material of pure titanium. All samples are firstly sterilized under high pressure and temperature by autoclave. After the thawing, the BMSCs are cultured in F12 medium (Hyclone, USA) supplemented with 10% FBS (Biological Industries, Israel) and antibiotics (Bayotime, China) in a humidified atmosphere of 5% CO₂ and 95% O₂ at 37°C for 4 passages. The cells are plated in a 96-well culture plates at the concentration of 2.5×10⁴ cell/ml for 48 hours, and the cell viability is detected by cell counting kit-8 (CCK-8; MCE, USA). Furthermore, the absorbance at 450 nm is measured by a KHBST-360 multi-detection microplate reader (Kehua, shanghai, China).

Table 2 Compositions of test media of m-SBF

Composition	Na ⁺	K ⁺	Mg ²⁺	Ca ²⁺	Cl ⁻	HCO ⁻³	HPO ₂ ⁻⁴	SO ₂ ⁻⁴
Concentration (mM)	142.0	5.0	1.5	2.5	103.0	10.0	1.0	0.5

In addition, BMSCs are cultured in 24-well culture plates at a concentration of 0.5×10^4 cell/ml for 48 hours, and the spreading morphology is detected by calcein (MCE, USA), in which the images are obtained by using a fluorescence microscope (Olympus, Japan) with a $40\times$ magnification. In order to detect the osteogenic cell differentiation, 0.1×10^4 cells/mL BMSCs are plated in 24-well plates and cultured with the F12 medium. The medium is replaced by osteogenic differentiation basal medium (Cyagen, China) after 24 hours, and the medium is changed every three days for 10–14 days. Matrix mineralization and bone-like nodule formation are detected by staining with xylenol orange (XO; Sigma-Aldrich, USA) according to specifications, and images of Mineralized matter are obtained using a fluorescence microscope (Olympus, Japan) with a $40\times$ magnification.

Statistical analyses in this study are performed using SPSS version 22.0 software, and GraphPad Prism 7. Data are expressed as the mean \pm SD. The differences among three or more groups are compared using the one-way analysis of variance (ANOVA) analysis followed by Tukey post hoc test. All tests are two-sided, and $P < 0.05$ is considered statistically significant.

3 Results and discussion

3.1 Effect of average power on LST of pure titanium

To realize the fabrication of high precision surface textures on pure titanium, effects of laser processing parameters on the precision of ablated surface textures by picosecond pulsed laser ablation are investigated. The single pulse energy E_p is determined by average power P_{avg} and repetition frequency f , as $E_p = \frac{P_{avg}}{f}$. Under the same average power, a higher repetition frequency leads to a smaller single pulse energy, which is beneficial for reducing heat affected zone (HAZ). Moreover, the ratio of laser beam spot overlap increases with the increase in repetition frequency, which

increases the surface integrity of ablated microgrooves without pits formed. Thus, the maximum repetition frequency of 1200 kHz is utilized to achieve the high efficiency and high precision laser micromachining. Therefore, the effects of average power and scanning speed on the precision of fabricated textures in terms of texture depth and width, as well as ablated surface quality, are investigated.

Average powers ranging from 1.8 W to 9 W with an interval of 0.6 W are considered to study the effect of average power on the LST of pure titanium. The other laser processing parameters are the same for each average power, as a repetition frequency of 1200 kHz, a scanning speed of 100 mm/s and a laser beam diameter of 30 μm . Figure 2a shows the image of ablated pure titanium sample, on which the formed microgrooves are visible for average power no less than 3 W. Figure 2b further shows the enlarged image of four neighboring microgrooves by optical microscopy, which demonstrates that individual grooves fabricated on pure titanium has good straightness and uniform width. In addition, Fig. 2b further presents the pitches between neighboring grooves. The errors of pitches between each other are 0.8%, 1.9% and 1.4%, which indicate the high machining accuracy of the LST of pure titanium.

Figure 3 further shows the microscopic morphology of individual microgrooves at different average powers of 5.4 W, 6 W, 6.6 W and 7.2 W. It is seen from Fig. 3a that for the average power of 5.4 W, the ablated microgroove surface with shallow depth is flat and smooth, and ablated surface has good quality accompanied with limited HAZ. For the average power of 6 W, both the depth and the width of ablated microgroove increase significantly, and the high quality of ablated microgroove surface is remained with no obvious cracks and irregular damages formed, as shown in Fig 3b. With the further increase of average power to 6.6 W and 7.2 W, the depth and the width of ablated microgrooves both increase, but the quality of ablated microgrooves surface deteriorates accompanied by the formation of considerable cracks and irregular damages at the microgroove edge, as shown in Fig. 3c, d.

Fig. 2 Morphology of microgrooves on pure titanium by LST under different average powers. (a) Global view; (b) Enlarged view

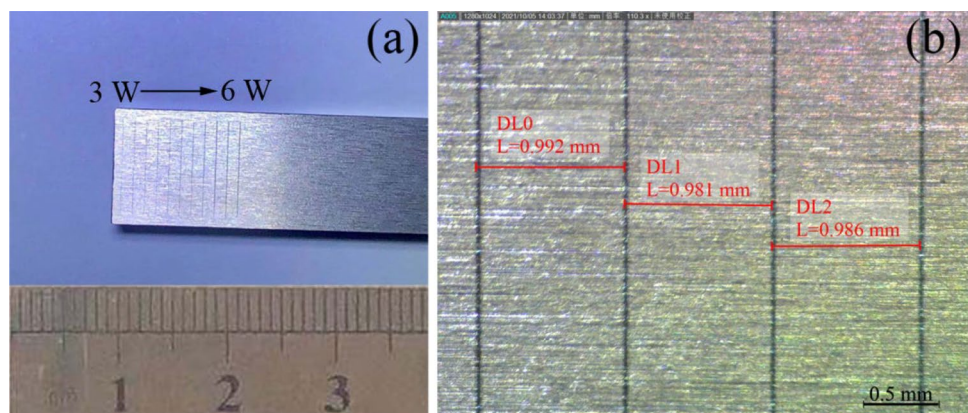
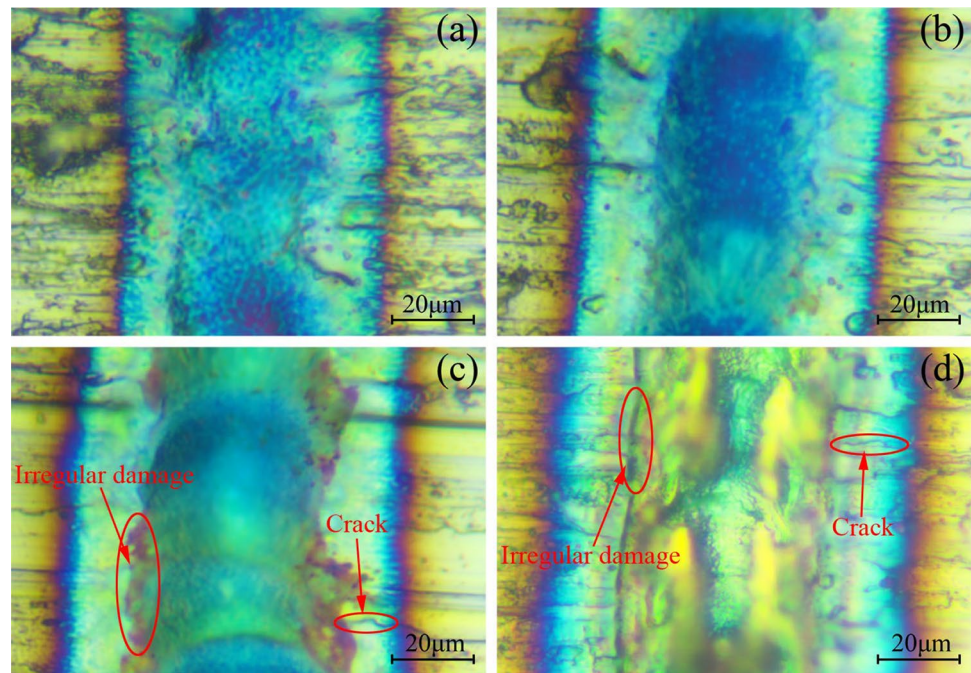


Fig. 3 Optical image of micro-groove profile under different average powers: (a) 5.4 W; (b) 6.0 W; (c) 6.6 W; (d) 7.2 W



Above results indicate that the applied average power has a significant effect on the microscopic morphology and quality of the microgroove. The material removal of pure titanium under low average power is mainly dominated by gasification [29], which corresponds to the weak ablation stage accompanied with shallow ablation depth of the microgroove. Since the reaction force in the ablated area is small, there is no cracking observed on the ablated surface. With the increase of average power, a strong ablation effect on the pure titanium material is produced, and the ablation removal effect of pure titanium material is further strengthened [30], which leads to increases in both the depth and the width of ablated microgrooves. However, when the average power is further increased, the pure titanium in the ablation area undergoes strong ablation with irregular material removal, which results in rough surface of ablated microgrooves. Part of deposited laser energy diffuses into the ablation microgrooves, leading to significant thermal damage of groove bottom. Due to the strong internal thermal stress, cracks and irregularities gradually appear on the edges of laser ablated microgrooves, resulting in poor surface integrity of ablated microgrooves and severe ablation damage.

The depth and the width of ablated microgrooves at different average powers are measured at three random locations by a white light interferometer. The variation of averaged depth and width of ablated microgrooves with average power is shown in Fig. 4a, b, respectively. It can be seen that both the depth and the width of microgrooves firstly increase with the increase in average power no higher than 6 W, indicating that the ablation process of pure titanium material has gradually changed from weak ablation to strong

ablation. Since the distribution of single pulse laser energy follows the Gaussian distribution in spatial domain, the increase in laser energy enhances the intensity of laser beam in the ablation area, which leads to an increase in the depth and the width of ablated groove up to an average power of 6.6 W. However, the depth decreases significantly with a further increase in average power higher than 6.6 W, as shown in Fig. 4a. Furthermore, the width decreases immediately for an average power above 6 W, which indicates that this is a critical value of average power for achieving a high ablation accuracy of pure titanium textures in terms of high groove quality and high precision morphology.

3.2 Effect of scanning speed on LST of pure titanium

To study the effect of scanning speed on the LST of pure titanium, scanning speeds ranging from 50 mm/s to 150 mm/s are considered. And the other laser processing parameters are the same for each scanning speed, as a repetition frequency of 1200 kHz, an average power of 6.0 W and a laser beam diameter of 30 μm . Figure 5a shows the image of ablated pure titanium sample, on which the formed microgrooves are visible for all the scanning speeds. Figure 5b further shows the enlarged image of four neighboring microgrooves by optical microscopy, which demonstrates that individual microgrooves fabricated on pure titanium has good straightness and uniform width for all the scanning speeds. In addition, Fig. 5b further presents the pitches between neighboring microgrooves. The errors of pitches between each other are 1.9%, 1.4% and 1.4%, which indicate the high machining accuracy of the LST of pure titanium.

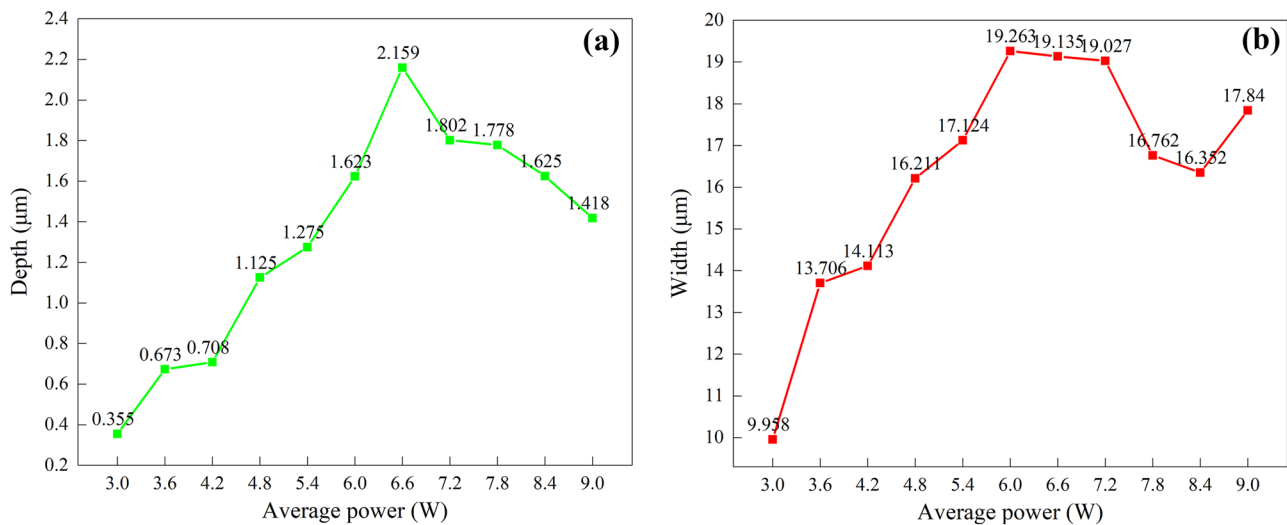


Fig. 4 Variations of (a) depth and (b) width of microgrooves with average power

Figure 6 further shows microscopic morphologies of individual microgrooves at different scanning speeds of 90 mm/s, 100 mm/s, 110 mm/s and 120 mm/s. Figure 6a shows that for the scanning speed of 90 mm/s, the ablated microgroove surface with large depth is rough, and the poor quality of ablated microgroove surface remains with obvious cracks and irregular damages. When the scanning speed is increased to 100 mm/s, the ablated microgroove surface is flat and smooth, and ablated surface has a good quality accompanied with limited HAZ, as shown in Fig. 6b. With the further increase in scanning speed to 110 mm/s and 120 mm/s, there are pits appeared on the ablated microgrooves, as shown in Fig. 6c, d. When the scanning speed is low, part of deposited laser energy diffuses into the ablation microgrooves, leading to significant thermal damage of groove bottom. Accompanied with the strong internal thermal stress, cracks and irregularities gradually appear on the edges of laser ablated microgrooves, resulting in poor surface integrity of ablated microgrooves and severe ablation

damage. With the increase in laser scanning speed, the pure titanium material in the ablation area undergoes weak ablation dominated by gasification, which leads to the decrease in the depth of microgrooves, and no crack is observed due to the small reaction force. In addition, the ratio of laser spot overlap is decreased with the increase in scanning speed, which results in the increase in the distance between adjacent laser spots accompanied with the formation of pits on the ablated microgrooves.

The depth and the width of ablated microgrooves at different scanning speeds are measured at three random locations by a white light interferometer. The variation of averaged depth and width of ablated microgrooves with scanning speed is plotted in Fig. 7a, b, respectively. It can be seen from Fig. 7a that the depth of microgrooves first decreases rapidly with the increase in scanning speed no higher than 70 mm/s, after which the depth remains unchanged for the scanning speeds between 70 mm/s and 100 mm/s. With the further increase in scanning speed, however, the depth

Fig. 5 Morphology of microgrooves on pure titanium by LST under different scanning speeds. (a) Global view; (b) Enlarged view

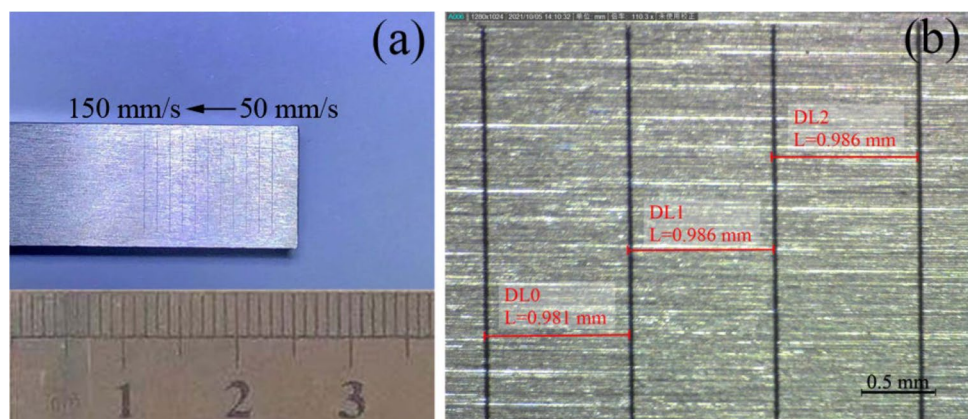
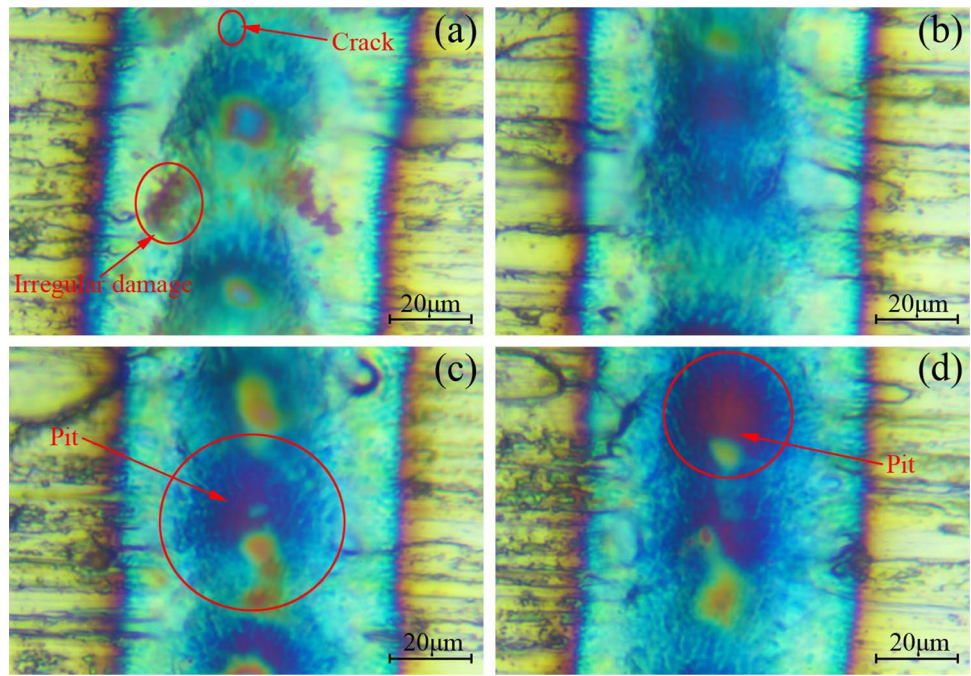


Fig. 6 Optical images of micro-groove profile under different scanning speeds: (a) 90 mm/s; (b) 100 mm/s; (c) 110 mm/s; (d) 120 mm/s



decreases dramatically. In contrast, Fig. 7b shows that the width of microgrooves is almost independent on scanning speed. Since the laser energy of single pulse follows the Gaussian spatial distribution, the change of scanning speed does not alter the laser intensity in the ablation area, which thus does not lead to the variation of microgroove width. Thus, the scanning speed of 100 mm/s should be used to achieve high accuracy of pure titanium textures in terms of high groove quality and high precision morphology.

3.3 LST of mesh-type texture on pure titanium

Above investigations on the dependence of LST of pure titanium on laser processing parameters indicate that the optimized average power and scanning speed is 6 W and 100 mm/s, respectively. Figure 8a shows SEM image of the ablated microgroove by using the optimized laser processing parameters, which demonstrates that the microgroove is straight and uniform in width. Figure 8b further shows SEM

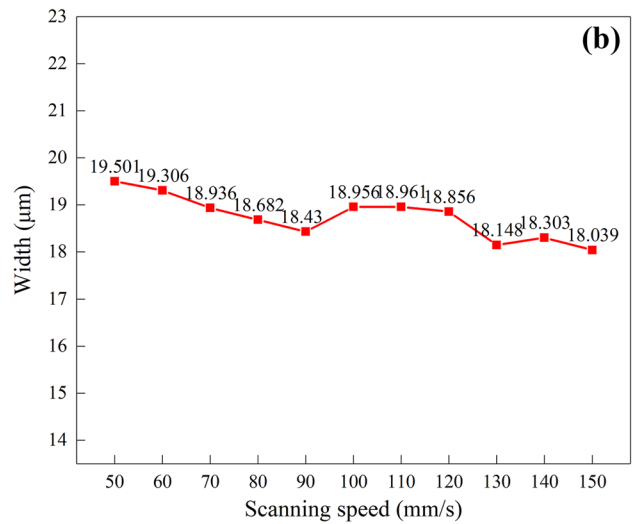
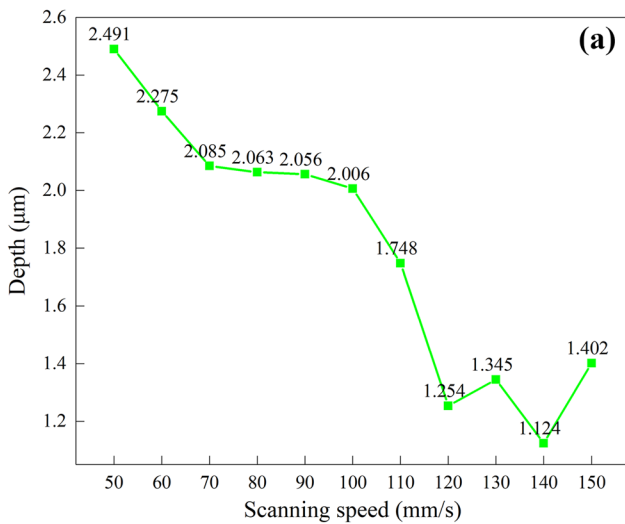


Fig. 7 Variations of (a) depth and (b) width of microgrooves with scanning speed

Fig. 8 SEM image of the ablated microgroove by using the optimized laser processing parameters. (a) Global view; (b) Enlarged view

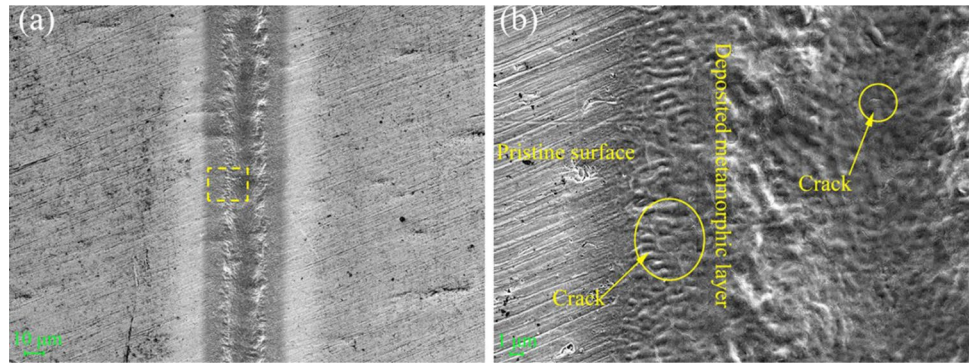


image of enlarged views of microgroove highlighted by the dash rectangle shown in Fig. 8a, which demonstrates minute cracks observed at bottom and edge of the microgroove caused by the redeposition of volatile titanium.

Therefore, the mesh-type texture with a width of 60 μm , a depth of 30 μm and a pitch of 200 μm is processed by LST using the optimized parameters. The strategy of cyclic scanning of complete mesh-type texture, rather than cyclic machining of single microgrooves, is adopted in the processing of surface textures to minimize the strong HAZ caused by the continuous diffusion of deposited laser energy into the microgrooves. Specifically, in the surface texturing process of the mesh-type textures, the laser beam firstly horizontally ablates parallel lines with pitch of 200 μm on the surface, and then, longitudinally ablates the parallel lines with pitch of 200 μm . And this process is repeated for 120 times to achieve a texture depth of 30 μm .

Figure 9a shows SEM image of the as-fabricated mesh-type textures on pure titanium, which demonstrates that each unit cell of the textures is evenly distributed and uniform in size. Figure 9b further presents SEM image of enlarged view of unit cell, which indicates that the unit cell of the textures is approximately square. However, the edge of the texture unit cell is rough and has a thick material accumulation layer, which can be attributed to the utilized strategy of cyclic scanning that provides sufficient time for the cooling and solidification of ablated material.

Fig. 9 SEM images of mesh-type textures fabricated on pure titanium: (a) Global view; (b) Enlarged view

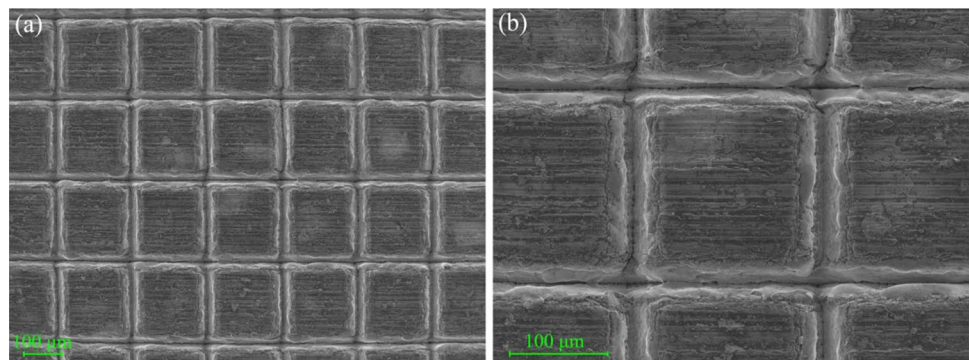
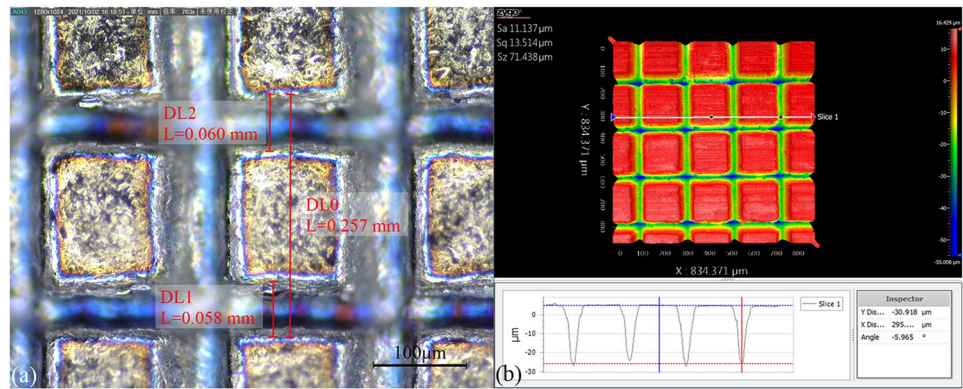


Figure 10a shows the optical image of the fabricated mesh-type textures, which demonstrates that the ablated microgroove surface is flat and smooth with no obvious cracks and edge breakages formed. It can be seen that the mesh-type texture has a width of 59 μm and a pitch of 198 μm . The error in width and pitch with the designed value is 1.0% and 1.6%, respectively. Figure 10b further shows the topography of mesh-type textures characterized by a white light interferometer, which demonstrates that the fabricated texture has good straightness and uniform distributions in shape, width, depth and pitch. Specifically, the average depth of microgrooves is approximately 30.9 μm , which has a deviation of 3% from designed value of 30 μm . Above low deviations in fabricated texture geometries from designed ones indicate the high machining accuracy of the LST of pure titanium.

3.4 Surface wettability of mesh-type textures on pure titanium

Figure 11a, b presents the evolution of DD water droplet profile on non-textured Ti surface and textured Ti-tex surface with time, respectively, which indicates that the contact angles for both surfaces decrease with time due to the decrease in surface tension with time. However, compared with the evolution of DD droplet profile on non-textured Ti surface, the evolution of the height and the occupied area of

Fig. 10 Geometry of mesh-type texture fabricated on pure titanium characterized by (a) optical microscope and (b) white light interferometer



DD droplet on textured Ti-tex surface is more significant. In addition, DD droplet on textured Ti-tex surface has smaller height and larger occupied area than that on non-textured Ti surface at the same time. Thus, the contact angle of DD droplet on textured Ti-tex surface is smaller than that on non-textured Ti surface.

Figure 12 plots variations of contact angle of DD water and m-SBF droplets with time on non-textured Ti surface and textured Ti-tex surface, which demonstrates the decrease in contact angle with time for each case, due to the decrease in surface tension. It can be seen from Fig. 12 that compared to the non-textured Ti surface, the decrease in contact angle with time for the textured Ti-tex surface is more pronounced for DD water and m-SBF, indicating a better wettability of the textured Ti-tex surface than the non-textured Ti surface. Surface wettability is known to be closely related with the surface topography produced by surface texture. According to Wenzel’s theory [31], since pure titanium is a hydrophilic material, the direction of

the capillary force is downward, which makes the liquid easily entering the textures to form a non-composite wettability model, leading to the increase in droplet diffusion in the groove. Thus, the initial hydrophilicity of the metal surface is amplified by the presence of surface textures. Furthermore, Fig. 12 indicates that the contact angle of DD water is slightly smaller than that of m-SBF, which is attributed to the higher concentration-induced higher surface tension of m-SBF than that of DD water.

The kinetics of droplet spreading on the non-textured Ti surface and the textured Ti-tex surface is further evaluated by fitting the contact angle-time curves according to Eq. (1) [32]:

$$y(x) = kx^n \tag{1}$$

where y and x represent the dynamic contact angle and time, respectively. k is empirical coefficients of initial contact angle, and n is spreading coefficient. As shown in Fig. 12, all the experimental data are fitted well by Eq. (1), with

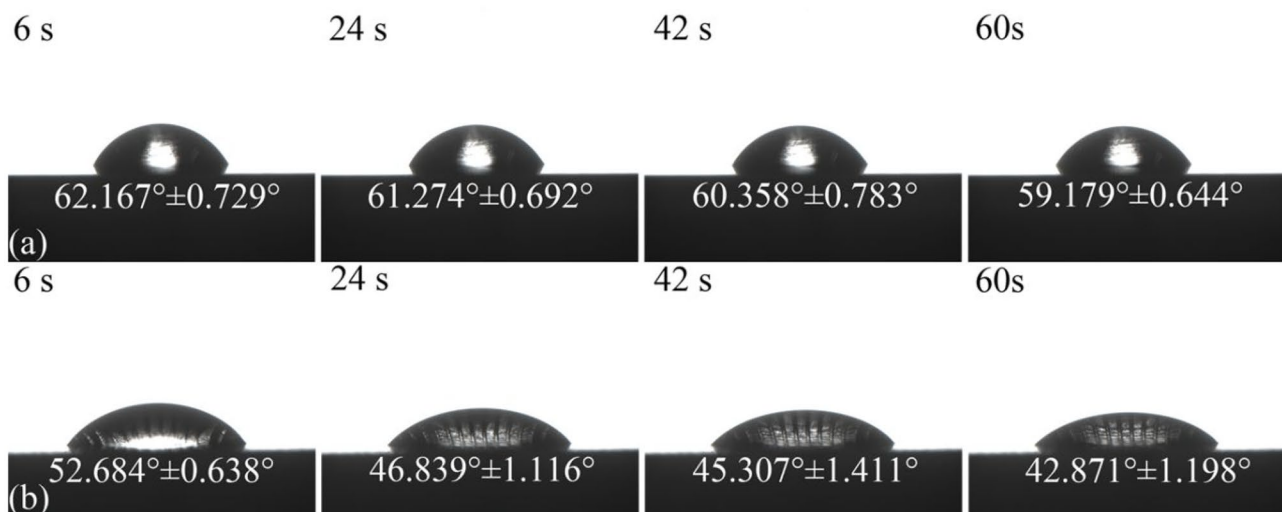
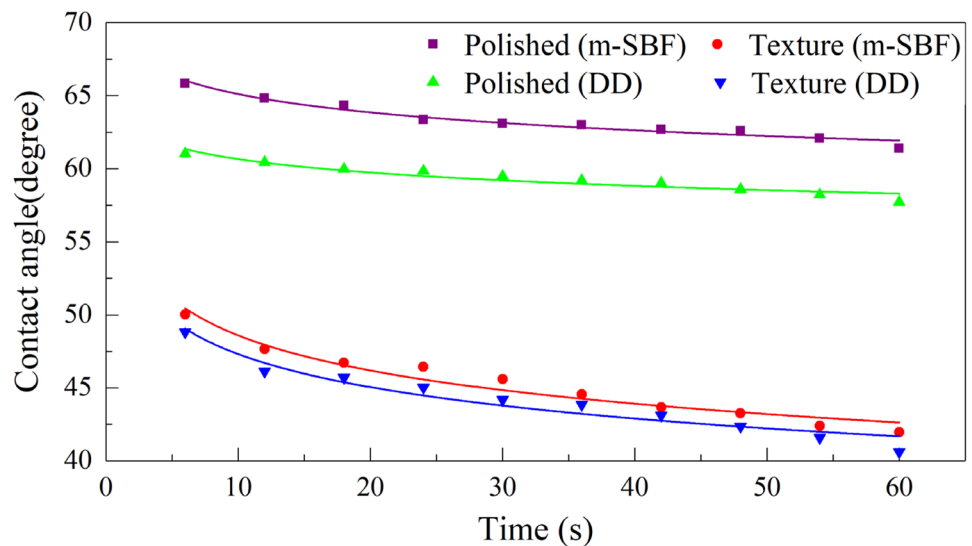


Fig. 11 Variations of contact angle of DD water droplet with time on (a) non-textured Ti surface and (b) textured Ti-tex surface

Fig. 12 Variations of contact angle with time for DD water and m-SBF droplets on non-textured Ti surface and textured Ti-tex surface



correlation coefficients (R^2) in the range of 0.90–0.96. Special attention is given to the value of droplet spreading coefficient n , and a higher value of n indicates a faster drop spreading kinetics [33, 34]. Table 3 lists derived values of n by fitting the experimental data shown in Fig. 12, which demonstrates that the spreading coefficient for the textured Ti-tex surface is higher than that of non-textured Ti surface for both DD water and m-SBF. Furthermore, the spreading coefficient of 0.051 for m-SBF droplet is approximately 11% higher than that of 0.046 for DD water. Thus, the as-fabricated mesh-type surface texture considerably affects the liquids spreading kinetics, due to the increase in the overall surface area and the surface free energy [35].

3.5 Biocompatibility of mesh-type textures on pure titanium

The viability of BMSCs is investigated 48 hours after cell seeding. Figure 13 shows that the viability of BMSC cells in the textured Ti-tex surface is significantly higher than that in the non-textured Ti surface, as the average cell viability in the textured Ti-tex surface (0.656 ± 0.106) is more than twice as much as in the non-textured Ti surface (0.277 ± 0.048). Figure 12 shows that the contact angle of textured surface is significantly lower than that of non-textured one, which is in line with the degree of cell proliferation and adhesion

Table 3 Spreading coefficient n calculated by fitting of experimental data

Sample	DD water		m-SBF	
	n	R^2	n	R^2
Non-textured	-0.02212	0.90	-0.028	0.96
Textured	-0.07079	0.93	-0.07317	0.95

shown in Fig. 13. This indicates that the cells grow better on the textured Ti-tex surface than that on the non-textured Ti surface, as the smaller contact angles of the textured Ti-tex surface are conducive to cell attachment and cell anchorages. Thus, the as-fabricated mesh-type surface textures are effective in promoting cell adhesion and proliferation.

The images of cell spreading and morphology are shown in Fig. 14, which demonstrates that the cells cultured on the non-textured Ti surface and the cells of control surface do not expand significantly after 48 hours of cell culture. On the contrary, the BMSCs cultured on the textured Ti-tex surface spread and are stretched broadly and uniformly on the surface. Furthermore, the growth status and distribution density of cells on the textured Ti-tex surface are more uniform than that on the non-textured Ti surface. Furthermore, the cells show better adhesion behavior on the textured Ti-tex surface than that on the non-textured Ti surface. Above

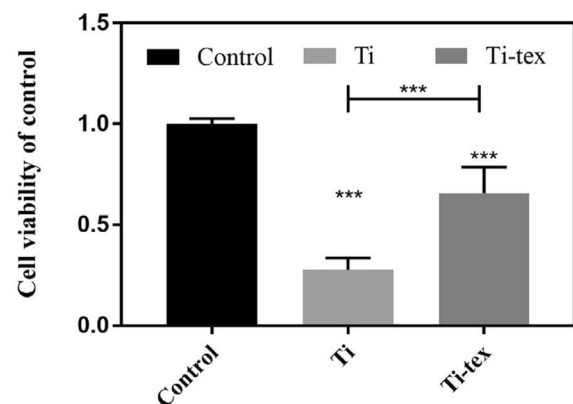
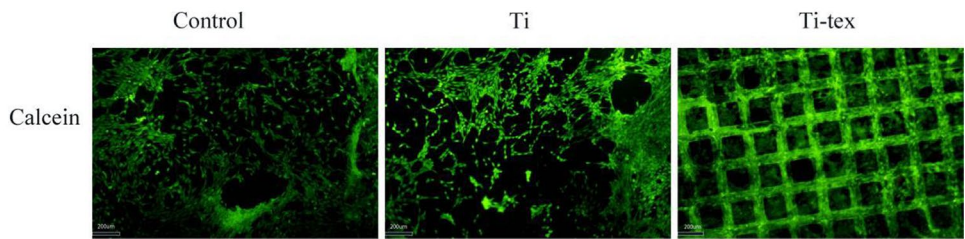


Fig. 13 Cell viability in the Control surface, non-textured Ti surface and textured Ti-tex surface. All data are expressed as the mean \pm SD ($n=3$). *** $P<0.01$

Fig. 14 Representative fluorescent images of cell spreading and morphology in Control surface, non-textured Ti surface and textured Ti-tex surface (n=3)



results indicate that the mesh-type surface textures have a strong impact on cell spreading, morphology and uniform distribution. When cells adhere to the microgroove surface, the mechanical effects accompanied with the microtopography stimulate actin in the cytoskeleton, which in turn causes the cytoskeleton to expand to contact along the microgroove [36]. At the same time, the cytoskeleton tends to be stretched along the same plane. When the cytoskeleton touches the microgroove boundary during the stretching process, it automatically alters the stretching direction to along groove direction, thus avoiding the extension out of the groove. Furthermore, while cells are stretched randomly on the non-textured Ti surface, the cell growth on the textured Ti-tex surface is along the groove direction, exhibiting a significant contact guidance phenomenon. Therefore, the as-fabricated mesh-type surface textures are effective in facilitating the uniform growth and distribution of BMSCs.

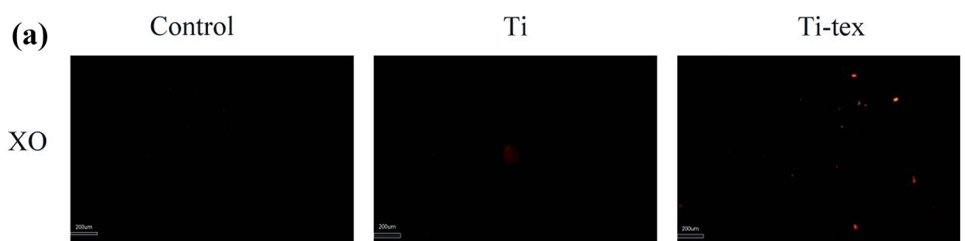
The differentiation of cells into an osteoblastic lineage is investigated 10-14 days after culturing. After induction of osteogenic differentiation of BMSC, a certain number of mineralized nodules are produced on the BMSCs surface. Figure 15a presents fluorescent images of mineralized nodules distributions for the three types of surfaces, which demonstrates that number of mineralized nodules for the textured Ti-tex surface is significantly higher than that for the non-textured Ti surface and the Control surface. Figure 15b

further quantifies the number of mineralized nodules for the three types of surfaces by XO-Fluorescence intensity, which indicates that the average fluorescence intensity in textured Ti-tex surface (408.25 ± 7.71) is the highest and is 230% higher than that of the non-textured Ti surface (123.58 ± 8.21). While bone mineralization occurs when calcium or phosphorus is precipitated in osteoblasts [37], thus the higher number of mineralized nodules for the textured Ti-tex surface than that for the non-textured Ti surface suggests that the mesh-type textures significantly facilitate the degree of differentiation of BMSCs into osteoblasts. Therefore, it indicates that textured Ti-tex surface can effectively promote the transformation of mesenchymal stem cells into osteoblasts, as well as the formation of mineralized nodules in the osteogenic induction environment. This can be attributed to the increased surface area and surface roughness by the surface texturing, which is beneficial for improving the adhesion, spreading and proliferation of cells.

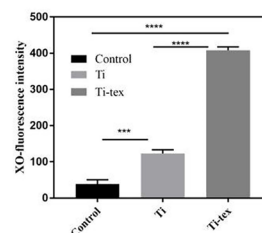
4 Summary

In summary, we investigate the fabrication and the evaluation of surface wettability and biocompatibility of mesh-type textures on pure titanium fabricated by picosecond pulsed laser ablation. In a careful investigation of the effect of laser

Fig. 15 Osteogenic cell differentiation. (A) Representative fluorescent images of osteogenic cell differentiation. (B) XO-Fluorescence intensity. All data are expressed as the mean \pm SD (n=3). ***P<0.01, ****P<0.001



(b)



processing parameters, we find an optimum of an average power at 6 W and of a scanning speed at 100 mm/s, which are selected for achieving a high accuracy of pure titanium textures in terms of high groove quality and high precision morphology. With the optimized laser processing parameters, precision mesh-type textures with a width of 60 μm , a depth of 30 μm and a pitch of 200 μm are fabricated on pure titanium. Subsequent evaluations of surface wettability and biocompatibility demonstrate that the as-fabricated surface texture is effective in facilitating droplet diffusion accompanied with decreased contact angle for both DD water and m-SBF, as well as in facilitating growth, spreading and differentiation of BMSC cells due to the better wettability of the textured surface.

Acknowledgements The authors gratefully acknowledge the National Natural Science Foundation of China (NSFC)-German Research Foundation (DFG) international joint research programme (51761135106), the Science Challenge Project (TZ2018006-0201-02).

Authors' contributions Junjie Zhang and Yu Liu conceived the project. Haoyu Li, Xin Wang and Binyu Wang established the device and performed the experiments; Marina Breisch, Alexander Hartmaier, Igor Rostotskiy and Vyacheslav Voznyy discussed the results. Haoyu Liu, Junjie Zhang, Alexander Hartmaier and Yu Liu wrote the paper. All authors read and approved the final manuscript for the submission.

Data availability The raw/processed data required to reproduce these findings cannot be shared at this time as the data also forms part of an ongoing study.

Declarations

Ethical approval Not applicable.

Consent to participate Not applicable.

Consent to publish Not applicable.

Competing interests The authors declare that they have no competing interests.

Reference

- Geetha M, Singh AK, Asokamani R, Gogia AK (2009) Ti based biomaterials, the ultimate choice for orthopaedic implants-A review. *Prog Mater Sci* 54:397–425
- Panjan P, Drnovšek A, Gselman P, Čekada M, Panjan M (2020) Review of growth defects in thin films prepared by PVD techniques. *Coatings* 10:447
- Shokrani A, Dhokia V, Newman ST (2012) Environmentally conscious machining of difficult-to-machine materials with regard to cutting fluids. *Int J Mach Tool Manuf* 57:83–101
- Durairaj S, Guo J, Aramcharoen A, Castagne S (2018) An experimental study into the effect of micro-textures on the performance of cutting tool. *Int J Adv Manuf Technol* 98:1011–1030
- Guo B, Sun J, Hua Y, Zhan N, Jia J, Chu K (2020) Femtosecond Laser Micro/Nano-manufacturing: Theories, Measurements, Methods, and Applications. *Nanomanufacturing and Metrology* 3:26–67
- Kurella A, Dahotre NB (2005) Surface modification for bioimplants: the role of laser surface engineering. *J Biomater Appl* 20:5–50
- Earl C, Castrejón-Pita JR, Hilton PA, O'Neill W (2016) The dynamics of laser surface modification. *J Manuf Process* 21:214–223
- Wang MZ, Wang CB, Kang JJ, Zhu LN, Yue W, Fu ZQ (2017) Effect of laser surface texture shape parameters on the tribological properties of titanium alloys. *China Surface Engineering* 30:71–77
- Kümmel D, Hamann-Schroer M, Hetzner H, Schneider J (2019) Tribological behavior of nanosecond-laser surface textured Ti6Al4V. *Wear* 422:261–268
- Xu JL, Tan WS, Hu ZR, Wang ST, Zhou JZ (2022) Study on High Temperature Friction and Wear Properties of Laser Surface Microtexture of TC4 Titanium Alloy. *Laser Optoelectron Prog* 59:1114002
- Cunha A, Serro AP, Oliveira V, Almeida A, Vilar R, Durrieu MC (2013) Wetting behaviour of femtosecond laser textured Ti-6Al-4V surfaces. *Appl Surf Sci* 265:688–696
- Li HY, Li LQ, Huang RR, Tan CW, Yang J, Xia HB, Chen B, Song XG (2021) The effect of surface texturing on the laser-induced wetting behavior of AlSi5 alloy on Ti6Al4V alloy. *Appl Surf Sci* 566:150630
- MacDonald DE, Markovic B, Allen M, Somasundaran P, Boskey AL (1998) Surface analysis of human plasma fibronectin adsorbed to commercially pure titanium materials. *J Biomed Mater Res* 41:120–130
- Conradi M, Kocijan A, Klobčar D, Godec M (2020) Influence of Laser Texturing on Microstructure, Surface and Corrosion Properties of Ti-6Al-4V. *Metals* 10:1504
- Xu Y, Li ZP, Zhang GQ, Wang G, Zeng ZX, Wang CT, Wang CC, Zhao SC, Zhang YD, Ren TH (2019) Electrochemical corrosion and anisotropic tribological properties of bioinspired hierarchical morphologies on Ti-6Al-4V fabricated by laser texturing. *Tribol Int* 134:352–364
- Zhou Y, Yang GZ, Zhang WJ, Hu J (2018) Investigating the effect of picosecond laser texturing on microstructure and bio-functionalization of titanium alloy. *J Mater Process Technol* 255:129–136
- Kumari R, Scharnweber T, Pfleging W, Besser H, Majumdar JD (2015) Laser surface textured titanium alloy (Ti-6Al-4V)-Part II-Studies on bio-compatibility. *Appl Surf Sci* 357:750–758
- Cunha A, Zouani OF, Plawinski L, Rego AMB, Almeida A, Vilar R, Durrieu MC (2015) Human mesenchymal stem cell behavior on femtosecond laser-textured Ti-6Al-4V surfaces. *Nanomedicine* 10:725–739
- Ataee A, Li Y, Brandt M, Wen C (2018) Ultrahigh-strength titanium gyroid scaffolds manufactured by selective laser melting (SLM) for bone implant applications. *Acta Mater* 158:354–368
- Yan M, Xu W, Dargusch MS, Tang HP, Brandt M, Qian M (2014) Review of effect of oxygen on room temperature ductility of titanium and titanium alloys. *Powder Metall* 57:251–257
- Duan WQ, Mei XS, Fan ZJ, Li JC, Wang KD, Zhang YF (2020) Electrochemical corrosion assisted laser drilling of micro-hole without recast layer. *Optik* 202:163577
- Yang Z, Sista S, Elmer JW, Debroy T (2000) Three dimensional Monte Carlo simulation of grain growth during GTA welding of titanium. *Acta Mater* 48:4813–4825
- Mishra S, Debroy T (2004) Measurements and Monte Carlo simulation of grain growth in the heat-affected zone of Ti-6Al-4V welds. *Acta Mater* 52:1183–1192
- Li JB, Liu S, Yu AB, Xiang ST (2018) Effect of laser surface texture on CuSn6 bronze sliding against PTFE material under dry friction. *Tribol Int* 118:37–45

25. Zhan XH, Yi P, Liu YC, Xiao PF, Zhu XY, Ma J (2020) Effects of single- and multi-shape laser-textured surfaces on tribological properties under dry friction. *Proc IME C J Mech Eng Sci* 234:1382–1392
26. Wang W, He YY, Zhao J, Mao JY, Hu YT, Luo JB (2020) Optimization of groove texture profile to improve hydrodynamic lubrication performance: Theory and experiments. *Friction* 8:83–94
27. Pratap T, Patra K (2020) Tribological performances of symmetrically micro-textured Ti-6Al-4V alloy for hip joint. *Int J Mech Sci* 182:105736
28. Li D, Neumann AW (1992) Contact angles on hydrophobic solid surfaces and their interpretation. *J Colloid Interface Sci* 148:190–200
29. Khosroshahi ME, Mahmoodi M, Saeedinasab H, Tahrir M (2008) Evaluation of mechanical and electrochemical properties of laser surface modified Ti-6Al-4V for biomedical applications: in vitro study. *Surf Eng* 24:209–218
30. Xu SZ, Chen Y, Liu H, Miao MM, Yuan XD, Jiang XD (2020) Femtosecond laser ablation of Ti alloy and Al alloy. *Optik* 212:164628
31. Wenzel RN (1936) Resistance of solid surfaces to wetting by water. *Ind Eng Chem* 28:988–994
32. Marmur A (1983) Equilibrium and spreading of liquids on solid surfaces. *Adv Colloid Interface Sci* 19:75–102
33. Wang XD, Zhang Y, Lee DJ, Peng XF (2007) Spreading of completely wetting or partially wetting power-law fluid on solid surface. *Langmuir* 23:9258–9262
34. Liang ZP, Wang XD, Lee DJ, Peng XF, Su A (2009) Spreading dynamics of power-law fluid droplets. *J Phys Condens Matter* 21:464117
35. Tiainen L, Abreu P, Buciumeanu M, Silva F, Gasik M, Guerrero RS, Carvalho O (2019) Novel laser surface texturing for improved primary stability of titanium implants. *J Mech Behav Biomed Mater* 98:26–39
36. Cai L, Zhang L, Dong J, Wang S (2012) Photocured biodegradable polymer substrates of varying stiffness and microgroove dimensions for promoting nerve cell guidance and differentiation. *Langmuir* 28:12557–12568
37. Zheng Q, Mao L, Shi Y, Fu W, Hu Y (2020) Biocompatibility of Ti-6Al-4V titanium alloy implants with laser microgrooved surfaces. *Mater Technol* 1–10

Publisher's Note Springer Nature remains neutral with regard to jurisdictional claims in published maps and institutional affiliations.